Unifying Frequency Combs in Active and Passive Cavities: Temporal Solitons in Externally Driven Ring Lasers

Unifying Frequency Combs in Active and Passive Cavities: Temporal Solitons in Externally Driven Ring Lasers

L. Columbo,[1,2,*] M. Piccardo,[3,4,*,†] F. Prati,[5] L. A. Lugiato,[5] M. Brambilla,[6] A. Gatti,[7,5] C. Silvestri,[1] M. Gioannini,[1] N. Opačak,[8] B. Schwarz,[8] and F. Capasso[4]

[1]*Dipartimento di Elettronica e Telecomunicazioni, Politecnico di Torino, 10129 Torino, Italy*
[2]*CNR-Istituto di Fotonica e Nanotecnologie, 70126 Bari, Italy*
[3]*Center for Nano Science and Technology, Fondazione Istituto Italiano di Tecnologia, 20133 Milano, Italy*
[4]*Harvard John A. Paulson School of Engineering and Applied Sciences, Harvard University, Cambridge, Massachusetts 02134, USA*
[5]*Dipartimento di Scienza e Alta Tecnologia, Università dell'Insubria, 22100 Como, Italy*
[6]*Dipartimento di Fisica Interateneo and CNR-IFN, Università e Politecnico di Bari, 70125 Bari, Italy*
[7]*Istituto di Fotonica e Nanotecnologie IFN-CNR, 20133 Milano, Italy*
[8]*Institute of Solid State Electronics, TU Wien, 1040 Vienna, Austria*

(Received 8 October 2020; accepted 29 March 2021; published 30 April 2021)

Frequency combs have become a prominent research area in optics. Of particular interest as integrated comb technology are chip-scale sources, such as semiconductor lasers and microresonators, which consist of resonators embedding a nonlinear medium either with or without population inversion. Such active and passive cavities were so far treated distinctly. Here we propose a formal unification by introducing a general equation that describes both types of cavities. The equation also captures the physics of a hybrid device—a semiconductor ring laser with an external optical drive—in which we show the existence of temporal solitons, previously identified only in microresonators, thanks to symmetry breaking and self-localization phenomena typical of spatially extended dissipative systems.

DOI: 10.1103/PhysRevLett.126.173903

Introduction.—The discovery of optical frequency combs [1,2] (OFCs) in high-Q ring microresonators filled with a Kerr medium, such as SiO_2, Si_3N_4, and diamond [3], and driven by an external laser beam activated worldwide attention on Kerr frequency combs (KFCs), because this avenue offers substantial potential for miniaturization and chip-scale photonic integration [4,5]. This technology has been applied to numerous areas, including coherent telecommunications and laser ranging [6,7]. It was recognized later [8,9] that the physics of KFCs corresponds very accurately to the model formulated in 1987 by the Lugiato-Lefever equation (LLE) [10]. This is a one-dimensional nonlinear Schrödinger equation in the presence of an external driving, linear damping, and detuning. The spontaneous formation of spatial patterns traveling along the cavity, described in the LLE, is the spatiotemporal equivalent of the frequency combs and governs their features [11]. By varying the frequency detuning θ of the pump laser injecting the microresonator a variety of spatial patterns can form [Fig. 1(a)], such as Turing rolls, breather solitons, and stable temporal solitons. A common feature of these spectra is that their envelope is bell shaped and can be approximated by a hyperbolic-secant function (sech) [3,12].

Recently, frequency comb spectra with sech-type envelope were also observed in ring quantum cascade lasers [QCLs, Fig. 1(c)] [13,14]. These are unipolar semiconductor lasers, first realized in 1994 [15,16], emitting in the midinfrared and terahertz regions of the electromagnetic spectrum. QCLs have attracted much attention, especially in midinfrared spectroscopy and sensing [17,18], thanks to their tunability via band-gap engineering and unique physical properties [19], such as ultrafast gain dynamics and strong resonant third-order nonlinearity. The study of ring QCLs operating in a unidirectional regime revealed a number of similarities with KFCs. It was found that the multimode laser instability is produced by the interplay of dispersive and nonlinear effects, as in the modulational instability (MI) of passive microresonators, and the number of localized structures appearing in the spatial patterns varies stochastically with the initial conditions [13]—a phenomenon known as multistability, also occurring in KFCs [3].

The similarity between the behaviors of these two disparate sources can be traced back to a precise formal analogy between their model equations, outlined by the scheme of Fig. 1. Indeed, it has been shown [13] that, under conditions of fast material dynamics and near-threshold operation, the dynamics of the ring QCL is well described by a complex Ginzburg-Landau equation (CGLE), where the two coefficients of the equation [Fig. 1(c)] are determined by the linewidth enhancement factor [20] (LEF or α factor) of the laser and by its group velocity dispersion (GVD) [21]. A CGLE was also formulated in Ref. [22], and analyzed in Ref. [23], in order to describe the 2D patterns

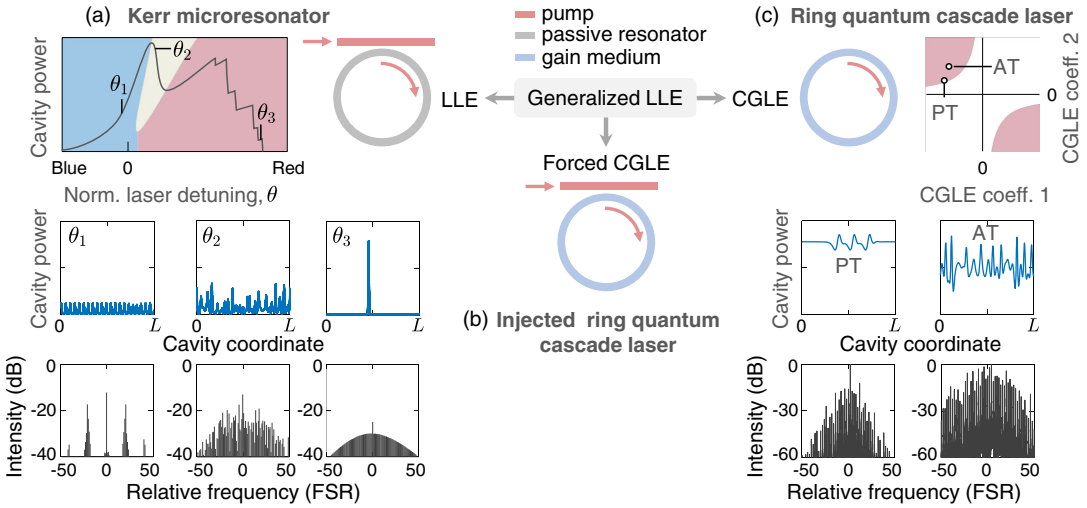

FIG. 1. Active and passive frequency comb sources: unification. (a) Schematic of a passive microresonator described by the LLE. The intracavity power depends on the pump laser detuning θ resulting in regions with different patterns: Turing rolls (blue), breather solitons (yellow), and stable temporal solitons (red). An example of different intensity distributions along the cavity and corresponding comb spectrum is given in each case. L denotes the cavity length. Images adapted from Ref. [9]. (b) Schematic of an intermediate system between the active and passive case consisting of a ring quantum cascade laser (QCL) injected by an external optical signal, which is described by a forced complex Ginzburg-Landau equation (CGLE). (c) Schematic of a unidirectional ring QCL described by the CGLE, which depends on two coefficients, related to the linewidth enhancement factor and group velocity dispersion of the laser. The ring laser can undergo a multimode transition in the red regions of the parameter space. The resulting dynamic behavior can be characterized by phase (PT) or amplitude (AT) turbulence.

arising in the transverse plane of the resonator due to the interplay of nonlinearity and diffraction. Such an equation can be regarded as the active counterpart of the LLE, which describes patterns in a driven passive resonator. Since the LLE, restricted to one dimension, also describes pulses traveling along the longitudinal axis of the resonator [24,25], it is natural to think of a similar equation for the active case.

These considerations led us to unify the two contexts of frequency combs in passive and active systems by formulating a generalized LLE, defined as the simplest equation that includes the passive and the active LLE as special cases. In turn, this step quite naturally leads to envisage a novel configuration; namely, a ring QCL with injected signal [Fig. 1(b)], which is studied in this work.

Generalized longitudinal LLE.—Let us consider the following equation that describes the spatiotemporal evolution of the envelope E of the electric field in an optical cavity

$$\tau_p \partial_t E = \overbrace{E_I}^{\text{driving}} + \overbrace{(-1 - i\theta_0)E}^{\text{damping-detuning}} + \overbrace{(d_R + id_I)\partial_z^2 E}^{\text{diffusion-dispersion}} + \underbrace{\mu(1 - i\Delta)(1 - |E|^2)E}_{\text{gain/loss, nonlinearity}}, \quad (1)$$

where t and z are the temporal and spatial coordinate along the cavity axis, in a reference frame moving at the light velocity in the cavity, and τ_p is the damping time of the cavity field. Electric fields are scaled [26,27] to present the equation in its simplest form (see Supplemental Material [28]). E_I is the amplitude of a coherent field injected in the cavity, which may or may not be present. In the second term, the -1 accounts for cavity losses and θ_0 is a detuning parameter. In the third term, the differential operator applied to cavity modes $\propto e^{ik_n z}E_n$ provides an algebraic term $-id_I k_n^2 E_n - d_R k_n^2 E_n$, whose imaginary part is associated with frequency dispersion while the real part (for $d_R > 0$) is a diffusion term that acts as a cutoff on the frequency spectrum. This term is connected to the reaction-diffusion mechanism responsible for pattern formation as described in Turing's theory of morphogenesis [29], where in our case the reaction is produced by all the other linear and nonlinear terms appearing in Eq. (1). Both terms arise from an adiabatic elimination of the material variables (Supplemental Material [28], which includes Ref. [30]) that takes into account the fast but not instantaneous response of the medium. In addition, d_I may contain the contribution of the GVD of a host medium. The fourth term describes the linear and nonlinear interaction of the electric field with the medium, as obtained by an adiabatic elimination of the material variables under the approximation $|E|^2 \ll 1$. In this term, μ is the unsaturated gain ($\mu > 0$) or absorption ($\mu < 0$) parameter. The coefficient of the nonlinearity Δ depends on the system under consideration, being, e.g., the atomic detuning for two-level media, or the LEF in the case of semiconductor lasers. In the latter case, it can also contain a contribution from the Kerr nonlinearity of the host medium.

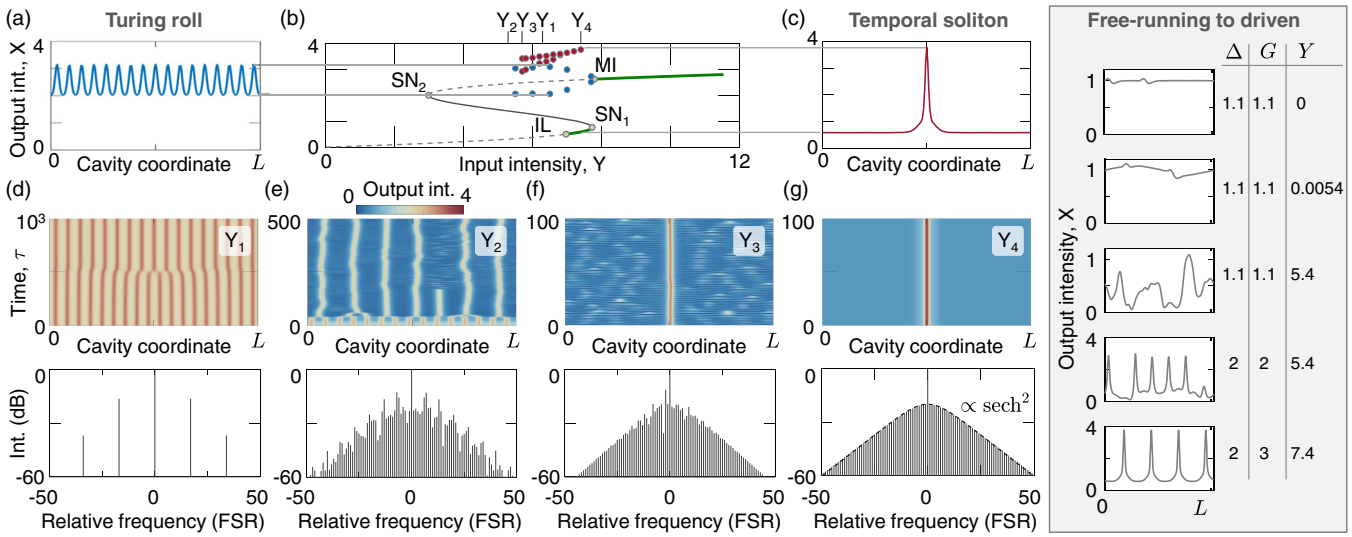

FIG. 2. Spatiotemporal dynamics of the injected ring quantum cascade laser. (a) 1D Turing rolls exhibiting periodic oscillations between two intensities, corresponding to a pair of blue dots in (b). (b) S-shaped curve of output intensity $X = |F|^2$ vs input intensity $Y = F_I^2$. Injection locking threshold (IL), saddle nodes (SN_1 and SN_2), modulation instability threshold (MI). Different segments of the curve can be stable (green line), unstable (dashed line), or not accessible (gray line). Blue and red dots correspond to Turing patterns and cavity solitons (CSs). (c) A CS with a pedestal and peak intensity corresponding to a point on the stable lower branch of the S-shaped curve and a red dot of (b), respectively. (d)–(g) Spatiotemporal plots and corresponding comb spectra of (d) Turing roll; (e) transition from Turing roll to non-stationary CSs; (f) CS on an unstable background; (g) stable CS. The input intensity is varied from Y_1 to Y_4 as marked in (b), i.e., first decreasing and then increasing again the intensity. Frequencies are relative to the central mode. Time is scaled to $\tau_p/|r|$, so that a smaller distance from threshold corresponds to a slower dynamics. The box shows from top to bottom localized structures emerging from phase instability in the free-running QCL [13], phase turbulence, amplitude turbulence, filamentation, CSs (see the full spatiotemporal plots in Supplemental Material [28]), when the laser is driven along an arbitrary trajectory across the parameter space.

In the following we will concentrate on the different limits of Eq. (1). Let us consider the passive and active case in order.

Passive case.—Here we assume that the medium is a weak absorber ($\mu < 0$, $|\mu| \ll 1$) with strong, negative atomic detuning ($\Delta < 0$, $|\Delta| \gg 1$) and large resonance curve bandwidth ($d_I \gg d_R$), so that the approximations $\mu(1 - i\Delta) \approx -i\mu\Delta$ and $d_R + id_I \approx id_I$ hold true and we obtain the LLE

$$\partial_\tau F = F_I - [1 + i(\theta - |F|^2)]F + i\partial_\eta^2 F, \tag{2}$$

with $\theta = \theta_0 + \mu\Delta$, $F = \sqrt{\mu\Delta}E$, $F_I = \sqrt{\mu\Delta}E_I$, $\tau = t/\tau_p$, and $\eta = z/\sqrt{d_I}$, where we assume that the dispersion is anomalous so that $d_I > 0$. In this case θ_0 must be taken as the cavity detuning $\theta_c = (\omega_c - \omega_0)\tau_p$, ω_c being the empty cavity frequency closest to the frequency ω_0 of the incident field.

Active case.—Here we assume that the medium is active and close to the lasing threshold ($\mu = 1 + r$, $|r| \ll 1$, above threshold for $r > 0$ and below for $r < 0$) and that $|E|^2$ has the same order of magnitude as $|r|$ so that the approximation $\mu(1 - |E|^2) \approx \mu - |E|^2$ is justified and we obtain an equation formally equivalent to a forced CGLE for

$$\partial_\tau F = F_I + \gamma(1 - i\theta)F - (1 - i\Delta)|F|^2 F + (1 + iG)\partial_\eta^2 F, \tag{3}$$

with $\gamma = r/|r|$, $\theta = (\theta_0 + \mu\Delta)/r$, $G = d_I/d_R$, $F = E/\sqrt{|r|}$, $F_I = E_I/|r|^{3/2}$, $\tau = |r|t/\tau_p$, and $\eta = z\sqrt{|r|/d_R}$. The relevant parameter is the detuning of the frequency ω_0 of the injected signal with respect to the frequency ω_L of the solitary laser. We show (Supplemental Material [28]) that this is given by $(\omega_L - \omega_0)\tau_p = r(\theta - \Delta)$.

In the Supplemental Material [28] we show that an equation identical to Eq. (3) can be derived from a full laser model for a QCL with coherent injection in the limit of ultrafast carriers and in proximity of the lasing threshold. In this case we have $\gamma = 1$ and

$$\Delta = \alpha + \beta, \qquad G = \alpha + \zeta, \qquad \zeta = -(1 + \alpha^2)\frac{\tilde{c}\tau_p}{2\tau_d^2}k'', \tag{4}$$

where α is the linewidth enhancement factor (LEF) [31], β and k'' are the Kerr and the GVD coefficient, respectively, of the host medium, while $\tilde{c}$ and τ_d are the group velocity of light in the medium and the polarization dephasing time in

the QCL with group index n. In this case $\theta_0 = \theta_c - \mu\beta$ and, therefore, $\theta = (\theta_c + \mu\alpha)/r$.

Above threshold and without an injected field Eq. (3) with $\theta = 0$, $\Delta = c_{\mathrm{NL}}$ and $G = -c_{\mathrm{D}}$ coincides with the CGLE in Refs. [13,32].

The dynamics of the electric field in the transverse plane of a similar system, i.e., a class-A laser with injected signal, was studied in Ref. [33] using an equation like Eq. (3), with the second order derivative along η replaced by the transverse Laplacian with a purely imaginary coefficient and $\Delta = 0$. Equation (3) with $\Delta = G = \alpha$ was already successful in describing the formation of phase solitons occurring in a driven bipolar semiconductor ring laser with a meter-size extended cavity [34]. Besides the ring geometry considered here, a connection between QCLs and the LLE was also established recently in the case of Fabry-Perot devices [35].

Temporal cavity solitons without background in a passive microcavity coupled with an amplifying fiber loop were demonstrated in [36]. This system cannot be described by the generalized LLE because it requires two coupled equations.

The injected ring QCL.—When an external coherent field is injected into the QCL [Fig. 1(b)], the generalized LLE describing this configuration encompasses two more control parameters: the external field intensity and frequency. Moreover, the injection of an external field allows the stationary and homogeneous solution to assume an S shape, as shown by Fig. 2(b)—a phenomenon known as optical bistability, occurring also in passive Kerr microresonators. In the active case above threshold only a segment of the lower branch of this curve is stable, and this occurs between the injection locking (IL) point, where the lasing frequency is locked to the injected field, and the turning point SN_1 [green segment in Fig. 2(b)]. Part of the upper branch of the curve is affected by a MI—a spontaneous symmetry breaking mechanism producing intensity patterns characterized by a high degree of spatial correlation [Fig. 2(d)], or else spatiotemporal turbulence [37]. As in passive microresonators, the S shape of the stationary curve creates conditions favorable for the generation of temporal solitons, referred to also as cavity solitons (CSs), i.e., dissipative localized structures formed inside an optical resonator. These conditions correspond to having an interval of input intensities in which the upper branch of the S curve is modulationally unstable and coexists with a stable homogeneous state in the lower branch.

In this situation the system might form a localized pattern emerging from the MI on a uniform stable background, and eventually give origin to a CS [27] [see Figs. 2(c,g)]. These considerations guided our search for CSs (and the associated OFCs) in QCLs with injected signal and in particular the choice of an experimentally reasonable parameter set. Figure 2 shows the results of numerical simulations of Eq. (3), performed with the following parameters: $\gamma = 1$, $\theta = 4.7$, $\alpha = 2$, $\beta = 0$, $\zeta = 1$ ($\Delta = 2$, $G = 3$). By assuming $n = 3.3$, $\tau_p = 50$ ps, and $\tau_d = 60$ fs [13], our parameters correspond to a slight red detuning of the pump field, e.g., 0.9 GHz for a laser 10% above threshold, and the GVD calculated from Eq. (4) turns out around -300 fs^2/mm, a realistic value for QCLs [38]. The S-shaped curve calculated for the selected parameter set is shown in Fig. 2(b). Note that, while the plotted input and output intensity are comparable, the corresponding physical quantities are scaled to r^3 and r, respectively, so that the physical injected intensity is typically much smaller than the output one.

By varying the input intensity $Y = F_I^2$ [39], we observe the following scenario emerging from numerical integration [40] of Eq. (3). Starting on the high-intensity spatially uniform solution, stable to the right of the MI point, and progressively decreasing Y, a globally modulated pattern bifurcates from MI at $Y_{\mathrm{MI}} = 7.8$ [Fig. 2(a) shows the pattern for $Y_1 = 6.3$]. The bifurcation is by definition supercritical as the branch that bifurcates remains stable, down to about $Y = 5.4$. The modulated pattern corresponds to a 1D Turing roll [29] and its branch is indicated by the blue dots in Fig. 2(b), which mark the maximum and minimum intensity. The period of the spatial modulation of the roll pattern depends on Y. This feature makes the injected ring QCL particularly appealing, because the comb spacing can be tuned by simply changing the intensity of the injected signal, rather than by widely tuning its frequency as it was done for the control of the harmonic state in Fabry-Perot QCLs [41]. Figure 2(d), in fact, shows a simulation where a period-18 roll pattern (stable only at $Y = 6.4$), taken as an initial condition, spontaneously evolves to a stable period-17 roll when $Y = Y_1 = 6.3$.

Below $Y = 5.4$ the rolls become unstable and the system undergoes a spontaneous collapse of the roll pattern. It evolves into a number of nonstationary CSs sitting on a turbulent background, which corresponds to the unstable lower branch of the steady-state curve [Fig. 2(e), $Y_2 = 5.3$]. A further decrease of Y brings the system in a turbulent regime where any ordered structure disappears. Conversely, by starting from the nonstationary CS and increasing the input intensity in the interval $5.7 \leq Y < 7$ a single CS with turbulent background survives [Fig. 2(f), $Y_3 = 5.8$]. The background fluctuations cause a jitter in the soliton shape and intensity maximum. The range of fluctuations of the CS peak are traced by the pairs of red dots in Fig. 2(b). Finally, by following upwards the soliton branch in the interval $7 \leq Y \leq 7.4$ the pedestal of the single CS becomes stable corresponding to the lower uniform and stable branch of the steady-state curve, as expected, since $Y_{\mathrm{IL}} = 6.97$ [Figs. 2(c),2(g), $Y_4 = 7.4$]. The CS spatial shape and corresponding spectra, well approximated by a sech^2 envelope [Figs. 2(f),2(g)], do not change in time. We note that CSs are not only predicted by our reduced model, but are also observed in our full dynamical model of the

QCL [see Eqs. (S1)–(S3) of the Supplemental Material [28], which includes Refs. [42,43]]. Moreover, we show that CSs emerge also when transitioning from the free-running [13] to driven case, when an appropriate path is swept in the multidimensional parameter space (Fig. 2, box).

The most appealing features of CSs, from the applicative viewpoint, are multistability, independence, and plasticity. The CSs reported here are (a) stable versus the considerable fluctuations such as those shown in the background of Fig. 2(f); (b) intrinsically multistable so that the injection of short pulses allows to excite multiple CSs (see Supplemental Material [28], which includes Ref. [44], for related simulations).

Conclusions.—The generalized LLE introduced in this work makes it possible to connect for the first time from a formal viewpoint Kerr microresonators and QCLs. The injected ring QCL is a direct result of this unification opening a pathway for the realization of new spatiotemporal patterns in QCLs such as Turing rolls and CSs, previously restrained to Kerr combs. The CS emerging from a CW input field demonstrate the possibility of generating high-contrast short pulses in this device. Although this result comes as a surprise, as it has long been thought that the ultrafast dynamics of QCLs should strongly suppress amplitude modulation [45] in the absence of a radiofrequency modulation of the gain [46], here we have shown that a short pulse regime is possible, thanks to soliton formation triggered by a compensation between dispersion and nonlinear self-phase modulation associated with finite LEF in a resonator with gain driven by an external CW optical signal. In Ref. [34] this requirement was fulfilled using a long external cavity (≈1 m) and a standard semiconductor bipolar laser with nanosecond gain recovery time. In this work we showed that unipolar lasers (QCLs), having carrier dynamics 3 orders of magnitude faster, allow us to downsize the cavity length to the millimeter range, with significant impact on chip-scale frequency comb applications.

*These authors contributed equally to this work.
†piccardo@g.harvard.edu

[1] T. Udem, R. Holzwarth, and T. W. Hänsch, Optical frequency metrology, Nature (London) **416**, 233 (2002).
[2] D. J. Jones, S. A. Diddams, J. K. Ranka, A. Stentz, R. S. Windeler, J. L. Hall, and S. T. Cundiff, Carrier-envelope phase control of femtosecond mode-locked lasers and direct optical frequency synthesis, Science **288**, 635 (2000).
[3] T. J. Kippenberg, A. L. Gaeta, M. Lipson, and M. L. Gorodetsky, Dissipative Kerr solitons in optical microresonators, Science **361**, eaan8083 (2018).
[4] P. DelHaye, A. Schliesser, O. Arcizet, T. Wilken, R. Holzwarth, and T. J. Kippenberg, Optical frequency comb generation from a monolithic microresonator, Nature (London) **450**, 1214 (2007).
[5] B. Shen, L. Chang, J. Liu, H. Wang, Q.-F. Yang, C. Xiang, R. N. Wang, J. He, T. Liu, W. Xie, J. Guo, D. Kinghorn, L. Wu, Q.-X. Ji, T. J. Kippenberg, K. Vahala, and J. E. Bowers, Integrated turnkey soliton microcombs, Nature (London) **582**, 365 (2020).
[6] T. J. Kippenberg, R. Holzwarth, and S. A. Diddams, Microresonator-based optical frequency combs, Science **332**, 555 (2011).
[7] Y. K. Chembo, Kerr optical frequency combs: theory, applications and perspectives, Nanophotonics **5**, 214 (2016).
[8] Y. K. Chembo and C. R. Menyuk, Spatiotemporal Lugiato-Lefever formalism for Kerr-comb generation in whispering-gallery-mode resonators, Phys. Rev. A **87**, 053852 (2013).
[9] T. Herr, V. Brasch, J. D. Jost, C. Y. Wang, N. M. Kondratiev, M. L. Gorodetsky, and T. J. Kippenberg, Temporal solitons in optical microresonators, Nat. Photonics **8**, 145 (2014).
[10] L. A. Lugiato and R. Lefever, Spatial Dissipative Structures in Passive Optical Systems, Phys. Rev. Lett. **58**, 2209 (1987).
[11] L. A. Lugiato, F. Prati, M. L. Gorodetsky, and T. J. Kippenberg, From the Lugiato–Lefever equation to microresonator-based soliton Kerr frequency combs, Phil. Trans. R. Soc. A **376**, 20180113 (2018).
[12] S. Coen and M. Erkintalo, Universal scaling laws of Kerr frequency combs, Opt. Lett. **38**, 1790 (2013).
[13] M. Piccardo, B. Schwarz, D. Kazakov, M. Beiser, N. Opacak, Y. Wang, S. Jha, J. Hillbrand, M. Tamagnone, W. Chen, A. Zhu, L. Columbo, A. Belyanin, and F. Capasso, Frequency combs induced by phase turbulence, Nature (London) **582**, 360 (2020).
[14] B. Meng, M. Singleton, M. Shahmohammadi, F. Kapsalidis, R. Wang, M. Beck, and J. Faist, Mid-infrared frequency comb from a ring quantum cascade laser, Optica **7**, 162 (2020).
[15] J. Faist, F. Capasso, D. L. Sivco, C. Sirtori, A. L. Hutchinson, and A. Y. Cho, Quantum cascade laser, Science **264**, 553 (1994).
[16] J. Faist, *Quantum Cascade Lasers* (Oxford University Press, New York, 2013).
[17] A. Hugi, G. Villares, S. Blaser, H. C. Liu, and J. Faist, Mid-infrared frequency comb based on a quantum cascade laser, Nature (London) **492**, 229 (2012).
[18] G. Villares, A. Hugi, S. Blaser, and J. Faist, Dual-comb spectroscopy based on quantum-cascade-laser frequency combs, Nat. Commun. **5**, 5192 (2014).
[19] H. Choi, L. Diehl, Z.-K. Wu, M. Giovannini, J. Faist, F. Capasso, and T. B. Norris, Gain Recovery Dynamics and Photon-Driven Transport in Quantum Cascade Lasers, Phys. Rev. Lett. **100**, 167401 (2008).
[20] W. W. Chow and S. W. Koch, *Semiconductor-Laser Fundamentals* (Springer, New York, 1999).
[21] N. Opacak and B. Schwarz, Theory of Frequency-Modulated Combs in Lasers with Spatial Hole Burning, Dispersion, and Kerr Nonlinearity, Phys. Rev. Lett. **123**, 243902 (2019).
[22] L. A. Lugiato, C. Oldano, and L. M. Narducci, Cooperative frequency locking and stationary spatial structures in lasers, J. Opt. Soc. Am. B **5**, 879 (1988).

[23] W. Kaige, N. B. Abraham, and L. A. Lugiato, Leading role of optical phase instabilities in the formation of certain laser transverse patterns, Phys. Rev. A **47**, 1263 (1993).
[24] M. Haelterman, S. Trillo, and S. Wabnitz, Dissipative modulation instability in a nonlinear dispersive ring cavity, Opt. Commun. **91**, 401 (1992).
[25] F. Castelli, M. Brambilla, A. Gatti, F. Prati, and L. A. Lugiato, The LLE, pattern formation and a novel coherent source, Eur. Phys. J. D **71**, 84 (2017).
[26] L. Columbo, S. Barbieri, C. Sirtori, and M. Brambilla, Dynamics of a broad-band quantum cascade laser: from chaos to coherent dynamics and mode-locking, Opt. Express **26**, 2829 (2018).
[27] L. Lugiato, F. Prati, and M. Brambilla, *Nonlinear Optical Systems* (Cambridge University Press, Cambridge, England, 2015).
[28] See Supplemental Material at http://link.aps.org/supplemental/10.1103/PhysRevLett.126.173903 for additional derivations and numerical simulations.
[29] A. M. Turing, The chemical basis of morphogenesis, Phil. Trans. R. Soc. B **237**, 37 (1952).
[30] F. Prati, M. Brambilla, M. Piccardo, L. Columbo, C. Silvestri, G. M., A. Gatti, L. Lugiato, and F. Capasso, Soliton dynamics of ring quantum cascade lasers with injected signal, Nanophotonics **10**, 195 (2020).
[31] C. Henry, Theory of the linewidth of semiconductor lasers, IEEE J. Quantum Electron. **18**, 259 (1982).
[32] In Refs. [10] and [22] and in this Letter the field envelope E multiplies the factor $e^{-i\omega_0 t}$, whereas in Ref. [13] it multiplies the factor $e^{i\omega_0 t}$, so that the E which appears in Ref. [13] is the complex conjugate of the E which appears in this Letter.
[33] C. J. Gibson, A. M. Yao, and G.-L. Oppo, Optical Rogue Waves in Vortex Turbulence, Phys. Rev. Lett. **116**, 043903 (2016).
[34] F. Gustave, L. Columbo, G. Tissoni, M. Brambilla, F. Prati, B. Kelleher, B. Tykalewicz, and S. Barland, Dissipative Phase Solitons in Semiconductor Lasers, Phys. Rev. Lett. **115**, 043902 (2015).
[35] D. Burghoff, Unraveling the origin of frequency modulated combs using active cavity mean-field theory, Optica **7**, 1781 (2020).
[36] H. Bao, A. Cooper, M. Rowley, L. Di Lauro, J. S. Totero Gongora, S. T. Chu, B. E. Little, G.-L. Oppo, R. Morandotti, D. J. Moss, B. Wetzel, M. Peccianti, and A. Pasquazi, Laser cavity-soliton microcombs, Nat. Photonics **13**, 384 (2019).
[37] I. Aranson and L. Kramer, The world of the complex Ginzburg-Landau equation, Rev. Mod. Phys. **74**, 99 (2002).
[38] D. Kazakov, M. Piccardo, P. Chevalier, T. S. Mansuripur, Y. Wang, F. Xie, C. en Zah, K. Lascola, A. Belyanin, and F. Capasso, Self-starting harmonic frequency comb generation in a quantum cascade laser, Nat. Photonics **11**, 789 (2017).
[39] Taking F_I real merely sets the reference phase for the optical field.
[40] We specify that a stochastic noise term mimicking spontaneous emission in the system was included in all the simulations.
[41] M. Piccardo, P. Chevalier, S. Anand, Y. Wang, D. Kazakov, E. A. Mejia, F. Xie, K. Lascola, A. Belyanin, and F. Capasso, Widely tunable harmonic frequency comb in a quantum cascade laser, Appl. Phys. Lett. **113**, 031104 (2018).
[42] F. Prati and L. Columbo, Long-wavelength instability in broad-area semiconductor lasers, Phys. Rev. A **75**, 053811 (2007).
[43] H. Li, P. Laffaille, D. Gacemi, M. Apfel, C. Sirtori, J. Leonardon, G. Santarelli, M. Rosch, G. Scalari, M. Beck, J. Faist, W. Hansel, R. Holzwarth, and S. Barbieri, Dynamics of ultra-broadband terahertz quantum cascade lasers for comb operation, Opt. Express **23**, 33270 (2015).
[44] M. Brambilla, L. A. Lugiato, and M. Stefani, Interaction and control of optical localized structures, Europhys. Lett. **34**, 109 (1996).
[45] M. Piccardo, P. Chevalier, B. Schwarz, D. Kazakov, Y. Wang, A. Belyanin, and F. Capasso, Frequency-Modulated Combs Obey a Variational Principle, Phys. Rev. Lett. **122**, 253901 (2019).
[46] J. Hillbrand, N. Opacak, M. Piccardo, H. Schneider, G. Strasser, F. Capasso, and B. Schwarz, Mode-locked short pulses from an 8 μm wavelength semiconductor laser, Nat. Commun. **11**, 5788 (2020).